

ANNUAL REPORT

AWARD NUMBER: 99HQGR0200

CRUSTAL DEFORMATION IN THE SAN FRANCISCO BAY AREA

Paul Segall, Mark H. Murray, and Shelley Kenner
Stanford University, Geophysics Dept., Stanford CA 94305-2215
(650) 725-7241, x5-7344 (Fax), segall@pangea.stanford.edu
(650) 723-9594, x5-7344 (Fax), mhmurray@stanford.edu
<http://pangea.stanford.edu/deform>

PROGRAM ELEMENTS: I & II

KEY WORDS: GPS-Campaign, GPS-Continuous, Fault Dynamics, Fault Stress Interactions

INVESTIGATIONS UNDERTAKEN

The primary goal of this project is to synthesize the deformation field in northern California, with emphasis on the populated San Francisco Bay region. We are combining Global Positioning System (GPS), Geodolite trilateration, and very-long-baseline interferometry observations collected primarily from U. S. Geological Survey (USGS) and Stanford University field campaigns, and the Bay Area Regional Deformation (BARD) permanent GPS network in northern California. Combining these data will enable us to clarify the rates of interseismic strain accumulation on the principal Bay area faults: the San Andreas, Hayward, and Calaveras faults, and their extensions north of the San Francisco Bay. We are also analyzing deformation following major northern California earthquakes, including the 1906 San Francisco and 1989 Loma Prieta earthquakes, to better understand postseismic relaxation and stress transfer. Finally, time-dependent inversions and finite-element calculations will improve our understanding of the structure and rheology of the sub-seismogenic crust in the San Francisco Bay area.

During the past year, we have continued our efforts to combine the available geodetic data sets, primarily the continuous and campaign GPS observations in the Bay Area. Much of this effort went towards comparing positions solutions determined using GAMIT by the Berkeley Seismological Laboratory (BSL), and GIPSY by the USGS. These comparisons revealed a number of problems with combining solutions derived from these two methods. Therefore, in collaboration with W. Prescott (USGS), we are currently using the USGS GIPSY point positioning algorithms to reprocess all of the available data in a self-consistent method. In the following section we present results from other ongoing projects, including the determination of a broad-scale deformation field across northern California and Nevada from continuous GPS measurements, studies of postseismic deformation from the 1906 and 1989 earthquakes, and finite-element models of the 1906 postseismic deformation.

RESULTS

Deformation in Northern California and Nevada

We analyzed data from 49 permanent GPS stations in California, Oregon, and Nevada that have been operating for at least 0.8 years during a 5.9-year span from November 1993 to October 1999, including all stations in the Bay Area Regional Deformation (BARD) network (Murray et al., 1998a). Measurements collected on 2000 days during this interval were analyzed by the GAMIT software using distributed processing methods. We estimated the station velocities and their covariance from the combined daily coordinate solutions by tightly constraining the positions and velocities of 5 IGS stations to their ITRF96 values, while accounting for offsets and excluding non-linear motions introduced by equipment changes and other non-tectonic behavior. We converted the station velocities to a North America plate reference frame by added an angular velocity that minimizes the horizontal motions of a subset of the ITRF96 stations whose relative motions are consistent with rigid-body rotation at the 2 mm yr^{-1} level. The estimated relative baseline determinations typically have 2-4 mm WRMS scatter about a linear fit to changes in north and east components and the 10-20 mm WRMS scatter in the vertical component.

Average velocities for the longest running stations from BARD and other nearby networks are shown in Figure 1. To account for colored-noise error processes, such as monument wander, multipath, and atmospheric effects, we scaled the formal uncertainties according to the approximate expression given by Mao et al. (1999) for the total uncertainty of velocity as a function of both the white noise and flicker noise uncertainties appropriate for North American sites. This flicker noise model results in velocity uncertainties 6–12 times their formal uncertainties.

Stations in eastern Nevada show little motion relative to North America, whereas the station on the Farallon Islands, 30 km offshore near San Francisco, is moving at 46 mm yr^{-1} N 35°W . This is consistent with the motion predicted by NUVEL-1A for the Pacific plate (DeMets et al., 1994), indicating that the network spans nearly the entire deformation field associated with the plate boundary.

The San Andreas Fault system accommodates $\sim 35 \text{ mm yr}^{-1}$ parallel to the predicted plate motion across a 100-km wide zone near the coast. The remaining $\sim 11 \text{ mm yr}^{-1}$ of predicted plate motion is distributed across the Sierran-Great Valley, and Basin and Range province with significant velocity components normal to the predicted direction. This region can be divided into 3 relatively stable crustal blocks delimited primarily by seismicity patterns. The Sierran-Great Valley (SG) block is located between the SAF and a northwest trending seismicity belt between Lake Tahoe and Mount Shasta in eastern California. This seismicity belt is the western edge of the Basin and Range province, which we divide into eastern (EB) and western (WB) blocks about the Central Nevada Seismic Zone (CNSZ).

Our preferred kinematic model (Murray et al., in prep., 2000), assumes a single angular velocity for SG block, and a single Euler pole location, but different angular velocity rates for the EB and WB blocks. The WRMS misfits for the horizontal components are 1, 1, and 2 mm yr^{-1} for the EB, WB, and SG regions, respectively. Relative motion along the boundaries between the regions varies with position. Because EB and WB share the same Euler pole, relative motion is purely extensional across oblique longitudinal lines, which the CNSZ closely approximates. The predicted extension at $40^\circ\text{N}, 118^\circ\text{W}$ is 3 mm yr^{-1} N 75°W . The relative motion between WB and SG at $40^\circ\text{N}, 121^\circ\text{W}$ is 3 mm yr^{-1} N 45°W , approximately parallel to the seismicity trend, indicating the deformation is primarily right-lateral strike-slip. Deformation at both these boundaries is in general agreement

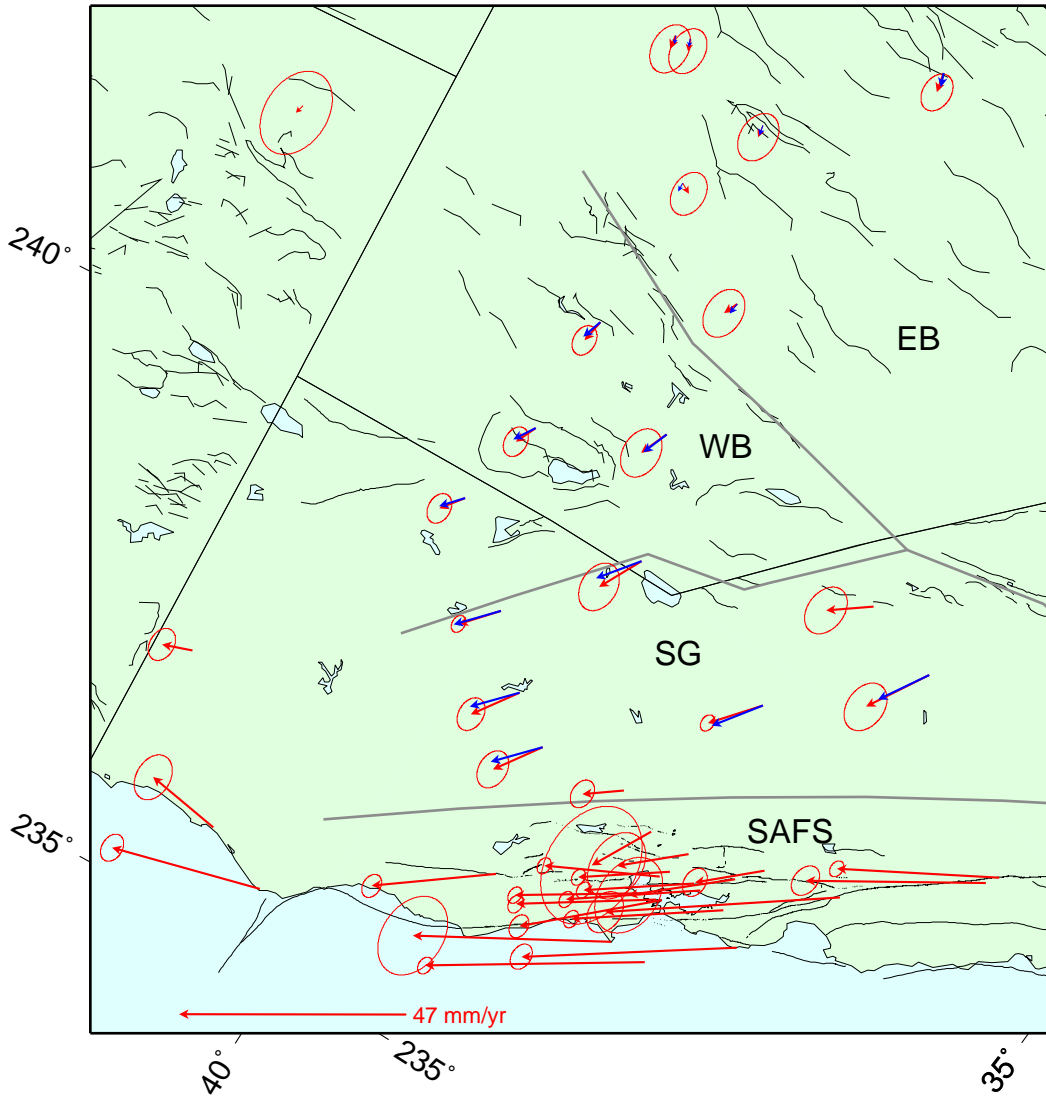


Figure 1: Observed (red) and modeled (blue) velocities relative to stable North America for stations in the BARD and nearby networks. Data from November 1993 to October 1999 was processed by the BSL using GAMIT software. Ellipses show 95% confidence regions, scaled by a white and flicker noise model, with the predicted Pacific–North America relative plate motion in central California shown for scale. The oblique Mercator projection is about the NUVEL-1 Pacific–North America Euler pole so that expected relative plate motion is parallel to the horizontal. Modeled velocities are from Euler pole determinations for the Sierran-Great Valley (SG), and west (WB) and east (EB) Basin and Range blocks. Velocities within the San Andreas fault system (SAFS) are estimated using two-dimensional models.

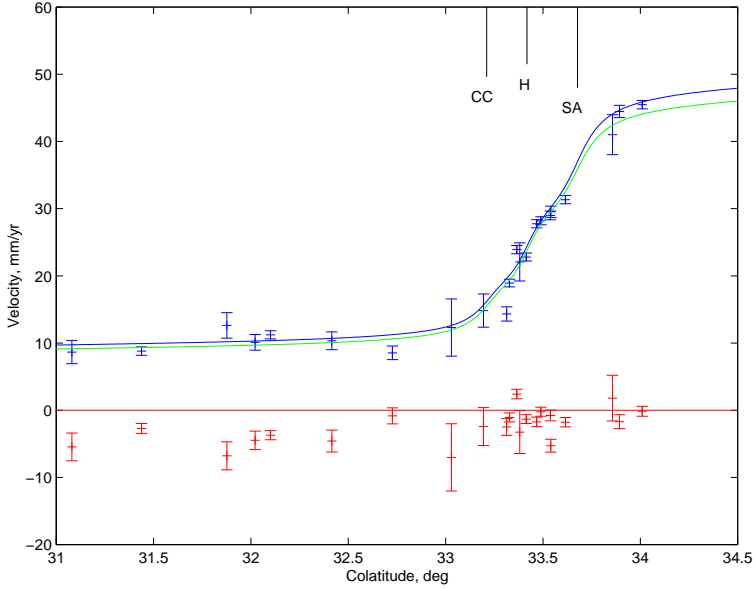


Figure 2: Velocities relative to the NUVEL-1A Pacific-North America Euler pole of stations located in a profile from western Nevada to the San Francisco Bay area. Observed velocities (crosses), with one standard deviation error bars, are perpendicular (red) and parallel (blue) to the predicted direction as a function of oblique colatitude from the Euler pole. The blue curve is the angular velocity and 3-fault backslip model. The green curve is the same model, assuming the NUVEL-1A rate on the Pacific plate. Vertical lines at top indicate location and relative depths of the San Andreas (SA), Hayward (H), and Calaveras/Concord (CC) faults.

with observed seismicity.

Motion of stations near the San Andreas fault system is approximately parallel to the NUVEL-1A predictions (Figure 2). Velocity components normal to this direction do not differ significantly from zero west of the SAF and are less than 5 mm yr^{-1} for sites between the SAF and Great Valley. The parallel velocity components vary in magnitude almost linearly by $\sim 35 \text{ mm yr}^{-1}$ across a 100-km wide zone near the coast, which previous studies show is consistent with interseismic strain accumulation on faults that are freely slipping except at shallow depths (Lisowski et al., 1991).

To model the observed deformation, we assume interseismic deformation is a superposition of long-term average rigid-body motions on either side of faults, and back-slip on shallow locked portions of faults. This approach is similar to the elastic dislocation model commonly used in subduction zone studies (Savage, 1983), except we express the long-term average motion using angular velocities. Given that the westernmost stations in our study form a roughly linear profile across the SAF system and their motions are predominantly parallel to predicted motion, we model interseismic strain accumulation using two-dimensional (anti-plane strain) screw dislocations. This method is described in more detail in Murray et al. (in prep, 2000).

Figure 2 shows the results using a model with 3 faults, corresponding to the San Andreas (SA), Hayward (H), and Calaveras/Concord (CC) fault strands. Given the high correlations associated with determining fault geometry and slip parameters in a parallel fault regime, we assume the fault locations are known from surface geology studies, and use locking depths derived from observed

seismicity. Estimated deep slip rates on SA, H, and CC faults are 19.2, 11.3, and 7.4 mm yr⁻¹, respectively, in reasonably good agreement with neotectonics studies (17 ± 4 , 9 ± 2 , and 5 ± 3 mm yr⁻¹, WGCEP, 1999). We are currently extending these methods to three dimensions to better characterize the complex geometry of faults in the San Francisco Bay area and will incorporate the more complete deformation field we are currently deriving using campaign GPS observations.

1989 Loma Prieta Earthquake Post-seismic Deformation

In Segall et al. (2000), we employ a modified version of the Network Inversion Filter to investigate time-dependent slip following the 1989 Loma Prieta earthquake. Previous analysis of Global Positioning System (GPS) and leveling data suggests afterslip on the Loma Prieta rupture as well as aseismic slip on a thrust fault northeast of the San Andreas fault which we identify with the Foothills thrust belt. We analyzed 173 daily GPS solution files at 62 stations collected from 1989.8 to 1998.3 (a total of 1,134 three-dimensional relative baseline determinations). The observed position changes are assumed to result from secular deformation, random benchmark motions, and temporally varying fault slip. The data reveal temporal variations in slip rate (Figure 3) but poorly resolve spatial variations in fault slip. The amount of temporal smoothing is estimated by maximum likelihood. Conditional on this estimate, reverse slip on the Foothills thrust decays from 45 ± 12 mm/yr immediately after the earthquake to zero by 1992. Reverse slip on the Loma Prieta rupture surface decays from 57 ± 11 mm/yr to zero by 1994. Right-lateral slip on the Loma Prieta rupture surface decays monotonically from 30 ± 10 mm/yr to zero by 1994. These results suggest that (1) triggered afterslip can occur off the main rupture zone on adjacent faults, (2) shallow afterslip dominated the postseismic deformation for the 8 years following the earthquake, and (3) postseismic slip on the Foothills thrust may account for a significant portion of its total slip budget.

1906 San Francisco Earthquake Postseismic Deformation

In Kenner and Segall (2000), we re-evaluate triangulation data from northern California following the 1906 San Francisco earthquake using improved methods [Yu and Segall, 1996] and combine the results with more recent geodetic data [Lisowski and Savage, 1992; Freymueller et al., 1999]. This significantly increases the temporal and spatial resolution of postseismic deformation following that event. We have calculated uniform shear strain-rates and average station velocities at Pt. Arena using data from 1906-07, 1929-30, and 1973-75 and for the Pt. Reyes-Petaluma arc using data from 1929-30, 1938-39, and 1960-61. With the addition of recent geodetic data, we infer an effective relaxation time for long-term, postseismic deformation following the 1906 earthquake of 36 ± 16 years (Figure 4). Inversion results allow us to investigate the corresponding decay in slip rates along a 10 km deep, 25 km wide, vertically oriented afterslip zone located below the trace of the San Andreas fault (Figure 5).

The Pt. Arena data can be reasonably fit with an accelerated deep afterslip model. Deformation in the Pt. Reyes-Petaluma arc (Figure 6) is clearly asymmetric with respect to the trace of the San Andreas fault, especially between 1929 and 1939. After inverting for the range of acceptable accelerated deep afterslip and horizontal detachment models, a detailed analysis using geologically reasonable geometries reveals that both model types have trouble explaining the spatial variations in the deformation field through time. In particular, accelerated deep afterslip models cannot reproduce the breadth of the observed deformation field to the northeast of the San Andreas fault.

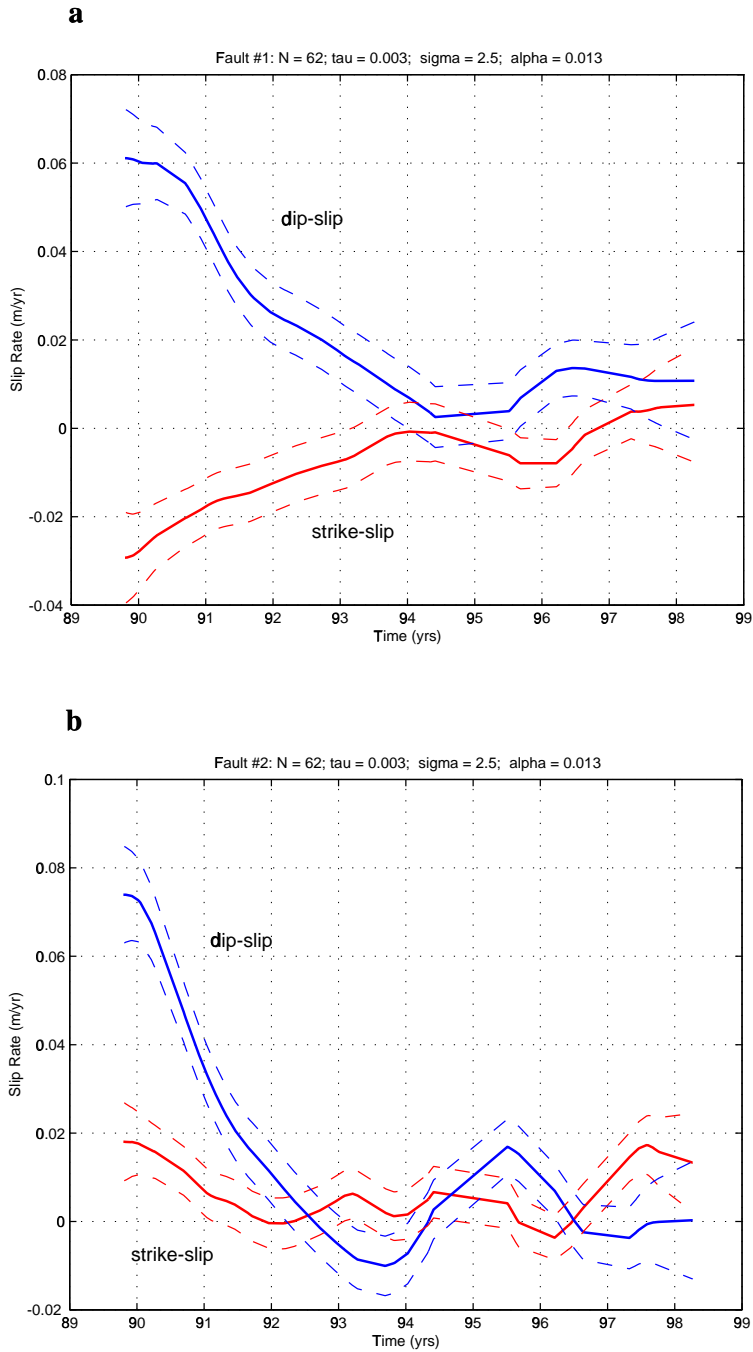


Figure 3: Estimated slip rate as a function of time. (a) Slip rate on the Loma Prieta fault. Positive dip slip is thrust, and right-lateral strike slip is negative. (b) Slip rate on the Foothills thrust fault. Dashed lines indicate plus and minus one standard deviation bounds.

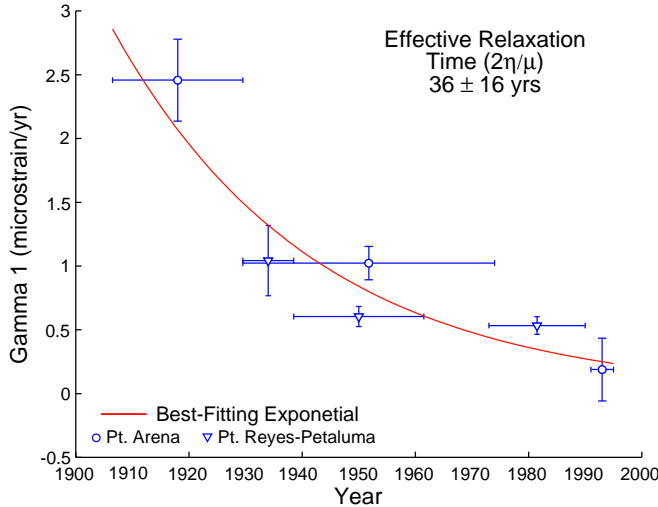


Figure 4: Evolution of uniform shear strain-rate with time since the 1906 San Francisco earthquake at Pt. Arena (circles) and Pt. Reyes (triangles). Vertical error bars give 1σ uncertainties. Horizontal error bars give the time between the first and last surveys included in the inversion. Strains have been rotated clockwise 20° and 10° , respectively, from north so that γ_1 represents the right-lateral shear strain-rate across that San Andreas fault.

As a result, more complex, time-varying deformation mechanisms are required to explain the Pt. Reyes-Petaluma arc observations.

Finite Element Models of Postseismic Deformation

Non-uniqueness is an inherent problem in modeling geodetic data. Comparison of fully spatial-temporal datasets with naturally time-dependent models can limit the number of possible solutions. We consider postseismic strain rate transients by comparing geodetic data from north of San Francisco Bay obtained between 1906 and 1995 [Kenner and Segall, 2000] to viscoelastic, anti-plane finite element models. Models include (1) an elastic plate over a viscoelastic half-space, (2) distributed shear within the lower crust, (3) discrete lower crustal shear zones within an otherwise elastic crust, (4) discrete shear zones embedded within a viscoelastic lower crust and (5) mid-crustal detachment surfaces. We vary, as applicable, locking depth (8, 12, 18 km), elastic crustal thickness (18, 25, 45, 60 km), lower crustal relaxation time (0.1–150 yrs), shear zone relaxation time (0.1–30 yrs), and shear zone width (0.2–4 km). For model types 3 and 4, dipping fault geometries are also considered [Parsons and Hart, 1999]. In total over 500 different finite element models were considered.

Models incorporating only distributed shearing (1,2) require very short relaxation times ($2^*\text{viscosity}/\text{shear modulus}$). For physically reasonable elastic plate over viscoelastic half-space models (1), the best-fitting models have relaxation times of 40 yrs, elastic thicknesses of 25 km, and fit all available data to within 4.3σ . The best distributed lower crustal shear models (2) have relaxation times of ≤ 5 yrs and a locking depth of 18 km. These models fit all available data to within 3.1σ . If the entire crust is elastic and discrete shear zones exist beneath each of the three sub-parallel faults in northern California (3), initially high strain rates immediately following the 1906 earthquake are

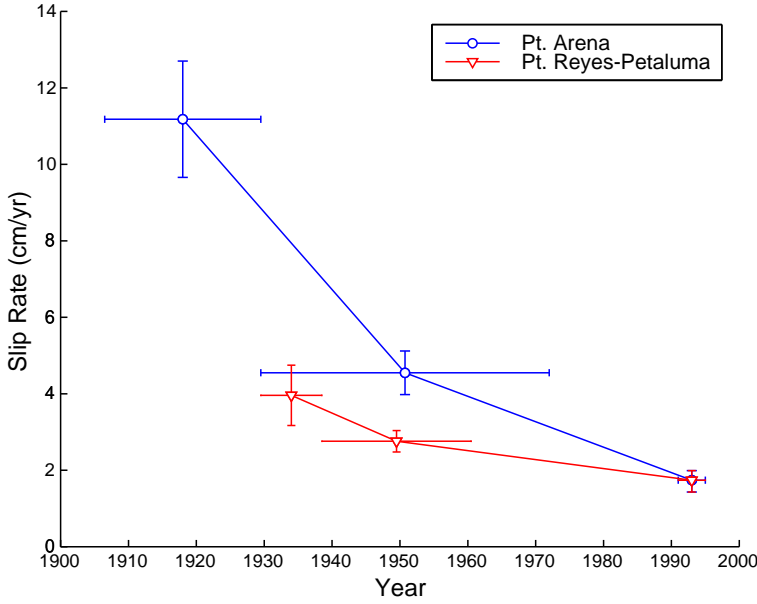


Figure 5: Slip-rate as a function of time since the 1906 San Francisco earthquake at Pt. Arena and the Pt. Reyes-Petaluma arc for a 25 km wide, deep accelerated afterslip zone whose top is located at 10 km depth. The slip-rate between 1991 and 1995 is from Freymueller et al. [1999] for all of northern California. Vertical error bars give 1σ uncertainties. Horizontal error bars give the time between the first and last surveys included in the inversion.

most reasonably fit with a locking depth of 12 km and elastic thickness greater than ~ 45 km. In the best case, all available data is fit to within 2.7σ . The case of discrete shear zones embedded within a viscoelastic lower crust (4) represents an intermediate case. Local minima in the misfit space represent models that approach distributed shear (2) and discrete shear zone (3) models. In the best case, all available data is fit to within 2.3σ (Figure 7), excluding outliers. The best detachment models fit the data to within 2.4σ . Dipping discrete faults do not significantly change the model fit to the data.

Geometrically reasonable elastic plate over viscoelastic half-space models (1) do a poor job predicting both the spatial distribution of deformation and variations in peak shear strain rate with time. While all other model types can emulate the observed decay of peak shear strain-rate at the San Andreas fault with time, the best-fitting distributed shear models (2) do a poor job predicting spatial variations in the deformation rate. Detachment models (5) yield reasonable results but recent findings from seismic reflection in northern California argue against the presence of a sub-horizontal detachment, in favor of discrete shear zones extending through the entire crust [Henstock et al., 1997; Parsons, 1998; Parsons and Hart, 1999; Zhu, submitted]. Our models incorporating discrete shear zones (3,4) are, therefore, more appropriate. Additionally, we conclude that the effective relaxation time seen in the postseismic geodetic data (Figure 4) is indeed effective, representing some net measure of deformation in a complex system. The best fitting discrete shear zone models (3,4) contain materials having at least two different relaxation times. One is extremely short, less than ~ 2 yrs, while the other is much longer (> 150 yrs). Alternatively, this finding may be indicative of prevalent non-linear material behavior in the lower crust. Finally, the

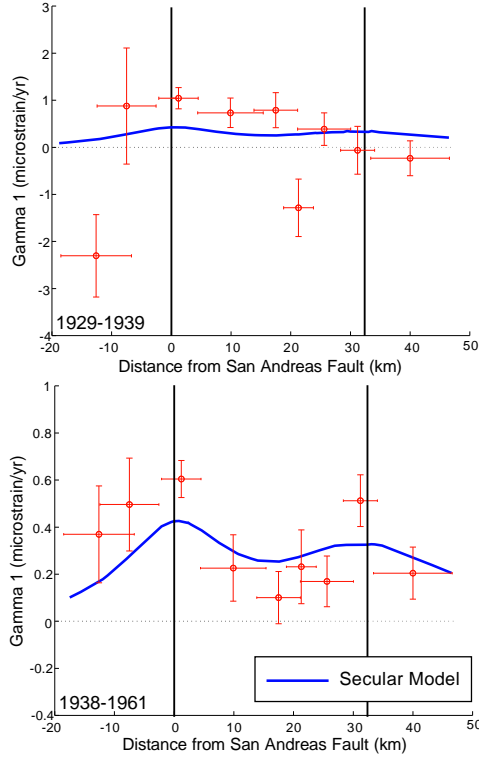


Figure 6: Right lateral engineering shear strain-rate across the San Andreas fault within the Pt. Reyes-Petaluma arc between 1929 and 1939 (top) and 1938 and 1961 (bottom). Vertical error bars give the 1σ uncertainty in the magnitude. Horizontal error bars give the lateral extent, in the fault parallel direction, of the subnet in which the calculation was made. The solid line gives expected results from the secular model of Bürgmann et al. [1994; 1997]. At the location of the Pt. Reyes-Petaluma arc the San Andreas fault is at an orientation of approximately N35°W. Note the different vertical scales. The heavy black lines denote the positions of the San Andreas and Rogers Creek faults.

effect of dipping faults is not significant to understanding postseismic perturbations to the deformation field following the 1906 earthquake.

NON-TECHNICAL SUMMARY

This project focuses on integration and modeling of geodetic measurements in the San Francisco Bay area. We combine previously collected Geodolite (precise laser distance measurements), Global Positioning System (GPS), and Very Long Baseline Interferometry (VLBI) measurements to determine the deformation field in the Bay area and to study how seismic stain accumulates on the principal faults. We also re-examine triangulation measurements made after the 1906 earthquake to study post-seismic relaxation and stress transfer, and perform time-dependent inversions and finite element calculations to study the fault geometry in the lower crust and stressing-rates on Bay area faults.

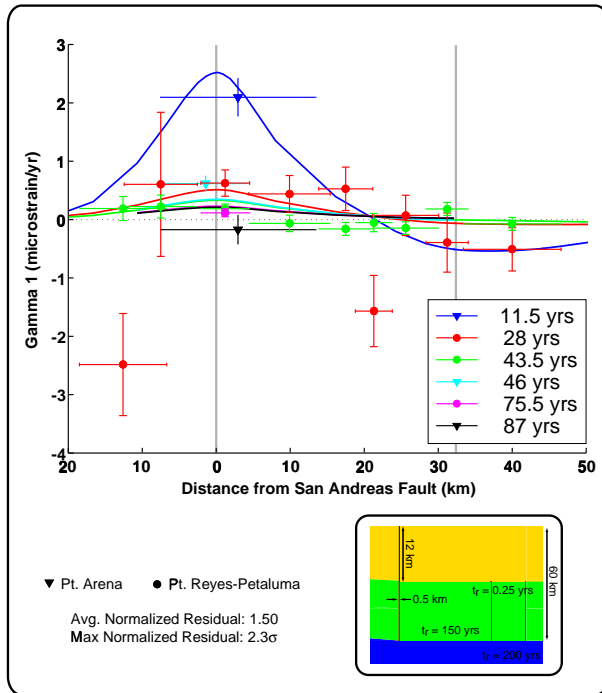


Figure 7: Best-fitting, geometrically reasonable model containing discrete shear zones within a Maxwell viscoelastic lower crust (4). The model has a seismogenic depth of 12 km. The shear zones, located beneath each of the three subparallel faults in the region, have a relaxation time of 0.25 yrs and extend to 60 km depth. The viscoelastic layer also extends to 60 km and has a relaxation time of 150 yrs. Below 60 km there is a Maxwell viscoelastic mantle with a relaxation time of 200 yrs.

REPORTS PUBLISHED

Freymueller, J. T., M. H. Murray, P. Segall, and D. Castillo, Kinematics of the Pacific-North American Plate Boundary Zone, northern California, *J. Geophys. Res.*, 104, 7419–7441, 1999.

Kenner, S. J., and P. Segall, Postseismic deformation following the 1906 San Francisco earthquake, *J. Geophys. Res.*, in press, 2000

Murray, M. H., R. Bürgmann, W. H. Prescott, B. Romanowicz, S. Schwartz, P. Segall, and E. Silver, The Bay Area Regional Deformation (BARD) permanent GPS network in northern California, *EOS Trans. AGU*, 79(45), Fall Meeting Suppl., F206, 1998a.

Murray, M. H., W. H. Prescott, R. Bürgmann, J. T. Freymueller, P. Segall, J. Svare, S. D. J. Williams, M. Lisowski, and B. Romanowicz, The deformation field of the Pacific-North America plate boundary zone in northern California from geodetic data, 1973–1989, *EOS Trans. AGU*, 79(45), Fall Meeting Suppl., F192, 1998b.

Murray, M. H., P. Segall, and B. Romanowicz, Continuous GPS measurements of Pacific-North America plate boundary deformation in northern California, 1993–1999, *Geophys. Res. Lett.*, in prep., 2000.

Segall, P., R. Bürgmann, and M. Matthews, Time-dependent triggered afterslip following the 1989 Loma-Prieta earthquake, *J. Geophys. Res.*, in press, 2000.

REFERENCES

- Bürgmann, R., R. Arrowsmith, T. Dumitru, and R. McLaughlin, Rise and fall of the southern Santa Cruz Mountains, California, deduced from fission track dating, geomorphic analysis, and geodetic data, *J. Geophys. Res.*, 99, 20,181–20,202, 1994.
- Bürgmann, R., P. Segall, M. Lisowski, and J. Svart, Postseismic strain following the 1989 Loma Prieta earthquake from GPS and leveling measurements, *J. Geophys. Res.*, 102, 4933–4955, 1997.
- DeMets, C., Effect of recent revisions to the geomagnetic reversal time scale on estimates of current plate motions, *Geophys. Res. Lett.*, 21, 2191–2194, 1994.
- Henstock, T. J., A. Levander, and J. A. Hole, Deformation in the lower crust of the San Andreas fault system in northern California, *Science*, 278, 650–653, 1997.
- Lisowski, M., and J. C. Savage, The velocity field in the San Francisco Bay area and the inferred depth of creep on the Hayward fault, Proceedings of the Second Conference on Earthquake Hazards in the Eastern San Francisco Bay Area , edited by G. Borchardt et al., *Spec. Publ. 113, Calif. Dept. of Conserv., Div. of Mines and Geol.*, pp. 39–44, Sacramento, 1992.
- Lisowski, M., J. C. Savage, and W. H. Prescott, The velocity field along the San Andreas fault in central and southern California, *J. Geophys. Res.*, 96, 8369–8389, 1991.
- Mao, A., G. A. Harrison, and T. H. Dixon, Noise in GPS coordinate time series, *J. Geophys. Res.*, 104, 2797–2816, 1999.
- Parsons, T., Seismic-reflection evidence that the Hayward fault extends into the lower crust of the San Francisco Bay area, California, *Bull. Seismol. Soc. Am.*, 88, 1212–1223, 1998.
- Parsons, T., and P. E. Hart, Dipping San Andreas and Hayward faults revealed beneath San Francisco Bay, California, *Geology*, 27, 839–842, 1999.
- Savage, J. C., A dislocation model of strain accumulation and release at a subduction zone, *J. Geophys. Res.*, 88, 4984–4996, 1983.
- Working Group on Earthquake Probabilities, Earthquake Probabilities in the San Francisco Bay Region: 2000 to 2030 – A Summary of Findings, *U.S. Geological Survey, Open-File Report 99-517*, 1999.
- Yu, E. and P. Segall, Slip in the 1868 Hayward earthquake from the analysis of historical triangulation data, *J. Geophys. Res.*, 101, 16,101–16,118, 1996.
- Zhu, L., Crustal structure across the San Andreas fault, southern California from teleseismic converted waves, *EPSL*, submitted, 1999.